Multiphase flow quantification using Computational Fluid Dynamics and Magnetic Resonance Imaging

Susithra Lakshmanan[1, 2], *Daniel Holland*[3], *Andy Sederman*[2], *Mikhail Gurevich*[4] *and Wes Maru* [1‡]

[1]Oil &Gas Measurement Limited, OGH, Ely, Cambridgeshire, UK
[2]Department of Chemical Engineering & Biotechnology, University of Cambridge, UK
[3]Department of Chemical & Process Engineering, University of Canterbury, Christchurch, NZ
[4]IMS Group, Moscow, Russia

Abstract

We investigated oil-water flow primarily with a view to quantify the mixing efficiency of a newly developed device with a Liquid Jet In Cross Flow (LJICF) configuration but also to predict the resulting flow regime and water droplet size distribution. Such devices are utilised in important applications such as liquid sampling in custody transfer, where the degree of homogeneity of the mixture affects the accuracy of the representative sample withdrawn and hence the oil transaction between producers and operators as well as taxation by governments. Despite their importance however, liquid-liquid flows under LJICF configurations have not featured as prominently in the literature as those of gas-liquid flows, resulting in a significant knowledge gap that needs to be addressed.

As part of a wide R&D programme at OGH, four experimental and calibration facilities are developed to conduct investigations in the general area of multiphase flows in a synergistic manner. These facilities are composed of: (a) small multiphase flow loop (SMPFL) primarily designed to fit in the University of Cambridge's Magnetic Resonance Imaging unit; (b) large multiphase flow loop (LMPFL), which is a scale up version of the SMPFL, (c) Flow Meter Calibration Loop (FMCL) to calibrate the flow meters for both the SMPFL and LMPFL, and (d) Heterogeneous High Performance Computing (HHPC) facility, where it is used to conduct and validate numerical experiments for any flow of interest based on new models developed in-house using the OpenFOAM® computational platform.

We also developed Magnetic Resonance (MR) techniques to be used in conjunction with the SMPFL. To quantify the water-cut, a chemically shift selective (CHESS) MR pulse sequence was developed. The CHESS technique saturates the unwanted signal from the oil component and only excites the water resonance. To verify that this sequence was quantitative, various water-oil mixture phantoms were prepared with water-cuts between 2.5% and 25%. By completely suppressing the oil spectrum peak, the water content can be readily quantified by integrating the signal intensity at each water-cut, where a quantitative comparison of the integrated signal intensity as a function of the known water-cut for the samples showed a linear relationship and demonstrate that the water cut is measured with an accuracy of approximately ± 0.2 %. The CHESS sequence was then combined with imaging sequences to enable visualisation of the water distribution in 2D. The developed technique is then used to study liquid-liquid flows and to characterise a novel mixing device that is developed by our partners to homogenise oil-water flows for custody transfer applications. The experimental results will be used to create accurate correlations as well as to validate our CFD simulation tools that are developed in-house on the OpenFOAM® computational platform.

‡ Corresponding author email address: wes.maru@oghl.co.uk

1 Introduction

Multiphase flows are very complex but also ubiquitous both in nature and in industry. Typically, multiphase flows occur in at least two-phases in the form of gas-liquid, gas-solid, liquid-liquid, liquid-solid or a combination of gas-liquid-solid flows. The complexity of such flows could be further compounded where any of the gas, liquid or solid phases each manifest as multicomponent fluids. For example, in the oil and gas industry, multiphase flows of oil-water or gas-oil-water with the presence of sand in either of the cases are very common.

Therefore, in the oil and gas industry, there is significant interest to understand multiphase flows not only to harness and efficiently utilise our resource to maintain the energy needs and economic development of current civilisation but also to develop smart solutions to maintain the health of our environment. To that end, we undertook the development of holistic approaches and integrated facilities that may allow us to predict, verify, quantify and control the evolution of multiphase flows. The current investigation is part of this large scale program but only considers liquid-liquid (or oil-water) flows, which have significant commercial importance in fiscal, allocation and custody transfer sampling applications. For example, in new oil-fields, the proportion of water-cut is relatively low (usually < 5%) while the water cut increases significantly as production declines and oil-fields mature. In both situations, it is important to quantify the water-cut relatively accurately.

The industry guide for the mixing, sampling, analysis (or calculation) and certification of a device to quantify the water-cut is described in the ISO 3171, API 8.2 and/or IP 6.2 (or IP 476:2002) standards - hereafter called Automatic Pipeline Sampling Standards (*APS Standards*). One of the key drivers to create and withdraw a representative sample so that the water-cut measurement will be accurate is homogenisation of the oil-water mixtures. Because, errors arising from poor mixed-ness could cost both industry and government millions of dollars a day in operational costs and revenue as well as in lost taxes. While our

main objective is to investigate a newly developed LJICF mixing system by our partners according to the *APS Standards*, we also took the liberty to posit the requirements for homogeneous mixing by focusing on the mechanistic behaviour of multiphase turbulence. Therefore, we will briefly address the practical issues of pipeline sampling from a point of jet break up and droplet distribution under non-steady flow conditions.

1.1 Automatic pipeline sampling

The *APS standards* provide a general guide covering all the essential steps of automatic pipeline sampling from the mixing process up to the sample analysis. The procedures for the sampling system including how to quantify the uncertainty of the measurements and its limitations are also provided. The sampling system certification proving test, which operates in a controlled or steady flow condition utilises a water injection procedure and is accompanied by the entire sequence of sampling as stipulated in the *APS standards*. Recently, Potten and Wright (2014) further elucidated the subject by providing historical data for a generation of their mixing systems. However, in real field operations, the flow is non-steady and so is the water cut. In this type of dispersed phase intermittency, although the type and frequency of the sampling equipment is believed to be crucial to gain an overall accurate result, this theory must be tested against experiment. Therefore, a review on the mechanistic behaviour of the jet mixing and droplet dispersion process is crucial as it will have significant effect on the mixing efficiency of the device to be used for custody transfer application.

1.2 Review of liquid-liquid flow diagnostics in pipes

Various techniques are employed by investigators to capture the behaviour of oil-water flows in pipes. A brief review on the most relevant techniques was provided by Lakshmanan et al (2015), which include visual observation, impedance probes, conductivity probes, particle imaging velocimetry (PIV), γ-ray Computer Tomography (CT), x-ray CT, wire mesh sensors and hot-film anemometers (Ismail et al. 2005; Xu 2007; Bieberle et al. 2013; Wang 2015).

Magnetic resonance (MR) imaging is also proving to be a useful tool for characterising single- and two-phase flow in pipes (Fukushima 1999; Elkins & Alley 2007; Gladden & Sederman 2013). MR has several advantages over the above techniques; it is completely non-invasive, can image optically opaque systems and can measure parameters including concentration, velocity, and diffusion. It is also possible to resolve each of these parameters spatially in one, two or three dimensions. However, there are some limitations of MR including a restricted sample geometry which is imposed by the need for a strong homogeneous magnetic field, an inability to image magnetic materials and difficulties associated with very heterogeneous materials (Fukushima 1999). MR techniques to study two phase flow include fast imaging techniques such as FLASH (Haase et al. 1986), RARE (Hennig et al. 1986), SPRITE (Sankey et al. 2009) and spiral EPI (Tayler et al. 2011). These techniques can be combined with velocity encoding to resolve the flow field (Tayler et al. 2012). When imaging liquid-liquid flows, it is important to resolve the signal from each phase independently. In this situation, chemical shift imaging (Maudsley et al. 1983) and chemical shift selective imaging (CHESS) (Götz & Zick 2003) are used. The acquisition time of these techniques can be reduced using advanced signal processing techniques like

compressed sensing (Holland & Gladden 2014). In this investigation, MR measurement is done using the SMPFL. However, in the section to follow, we first examine the mechanistic processes that may be responsible in achieving homogeneous mixing of liquid-liquid flows under LJICF configuration.

1.3 Jet mixing and droplet dispersion

LJICF configuration is one of the most common and efficient way of breaking up a liquid jet in to uniform droplets to create homogeneously dispersed flow in a wide range of operating conditions. Common examples and advanced applications of LJICF (or JICF in general) are smokestacks, volcanic plumes, atmospheric dispersion, oil spills, liquid fuel injection in scramjets and turbine blade film cooling. These have been investigated by many researchers (Clark 1964; Geery & Margetts 1969; Holdeman 1993; Mahesh 2012). Most studies of LJICF focus to predict and gain understanding of the jet trajectory but the subsequent jet break-up and the dispersion of droplets in the cross flow remains very complex and unexplored.

Recently, oil-water homogenisers that are used for custody transfer applications typically use LJICF configuration, often using multiple jets (Fernando & Lenn 1990). It is assumed, the trajectory of a single jet describes the extent to which the jet penetrates into the crossflow and also provides an estimate on how the droplets are dispersed with the flow. If sufficient turbulence is created, it gives rise to homogeneous mixing (Mahesh, 2012). However, there are various ways of defining and scaling the jet trajectory, mainly depending on the maxima of the local velocity, scalar mixing, or vorticity (Margason 1993; Smith & Mungal 1998; Mahesh 2012). Many studies have focused on single jets. However, multiple jets ensure better mixing and may also decrease the power requirements compared to if a single jet was to be used (Fernando & Lenn 1990; Wang et al. 1999). Most investigations on LJICF have been on gas-liquid flows and relatively little effort has been applied to study liquid-liquid flows. However, there are significant differences between the behaviour of gas-liquid and liquid-liquid flows under LJICF configuration. The liquid-liquid density ratio is two to three orders of magnitude higher than those of gas-liquid systems. There is also a relatively narrow band in the viscosity ratios of liquid-liquid systems than those of gas-liquid systems making the viscous dissipation significant. As such, liquid-liquid systems are more difficult to draw general conclusion compared to gas-liquid systems (Simmons and Azzopardi, 2001). Furthermore, the continuous phase in liquid-liquid system is much denser and more viscous than those of gas-liquid systems thereby resulting in slower settling velocity of droplets and having a higher propensity of dispersion. But, care should be taken when comparing liquid-liquid systems of varying densities and viscosities. In this case, there is a trade-off between energy input, to create jet break up and dispersion, and droplet suspension time. Contrary to the guidance from the *APS standards*, high viscosity and high density oils will provide longer suspension time for water droplets, maintaining its mixed-ness provided the stream velocity is not too low. Therefore, it is low density, low viscosity and low stream velocity conditions that are the worst case scenario in pipeline mixing as pointed out by Potten and Wright (2014). However, these authors didn't provide evidence on the performance of their mixing systems at very low stream velocities, as we will demonstrate later. However, to achieve the optimal homogeneity, the LJICF configuration problem has to be posed as an exercise to achieve a narrow droplet distribution that will remain suspended for a reasonable period but with minimal energy input and without an opportunity to create permanent emulsion. Of

course, this will be valid for relatively low water cut or dilute dispersed phase situations. For higher water cuts or dense dispersed phases, droplet collision and coalescence will complicate the dynamics (Valle, 1998; Trallero, 1995; Simons and Azzopardi, 2001) as well as the droplet size and its size distribution. The current jet trajectory formulations (Clark 1964; Geery & Margetts 1969; Holdeman 1993; Mahesh 2012) are empirical correlations for gas-liquid systems and can't be used for liquid-liquid systems under LJICF configurations. A novel multi-jet homogeniser was design on the basis of a jet penetration model for a single jet in a liquid-liquid system under LJICF configuration. In this model, the jet penetration was characterised (Lakshmanan et al, 2015) by:

$$\frac{x_n}{d_J} = \left(\frac{y_n}{d_J}\right) r^{\beta} + \left[\frac{C_D(\mathrm{Re}_{J\infty})}{J_m} - \frac{\mathrm{Ga}_J}{2\mathrm{Re}_J^2}\right]\left(\frac{y_n}{d_J}\right)^2, \quad (1)$$

Where y_n and x_n represent the jet penetration into the cross flow and the jet trajectory length along the stream-wise direction, respectively, C_D is the drag coefficient due to a cylindrical liquid jet in cross flow as a function of the Reynolds number ($Re_{J\infty}$), which is based on the relative velocity of jet and stream, Re_J is the jet Reynolds number, $Ga_J = gd_J^3/v^2$ is the Galileo number as a relative measure of the gravitational and viscous forces affecting droplet settlement, $J_m = \rho_J u_J^2/\rho_\infty u_\infty^2$ is the important momentum flux ratio, with ρ_J and ρ_∞ representing the jet and stream densities, respectively; and $r = u_J/u_\infty$ is the jet-to-stream velocity ratio for non-stationary streams, β is a correlation parameter with a value ≥ 1. The measurement and prediction of jet break up and droplet size distribution of both gas-liquid and liquid-liquid systems under LJICF configuration is much more challenging (Fernando & Lenn 1990; Wang et al. 1999; Simmons and Azzopardi, 2001; Mahesh 2012). Recently, Bolszo et al (2014) considered a pure liquid and emulsion jet break up and droplet formation under LJICF configuration and provided a relation of the form:

$$\frac{D_{32}}{d_J} = A\left(\frac{x_n}{d_J}\right)^B {J_m}^C \mathrm{We_J}^D \mathrm{Re}_{J\infty}{}^E \quad (2)$$

Where D_{32} is the Sauter mean droplet diameter, We_J is the jet Weber number while A, B, C, D and E are empirical parameters that are dependent on the fluid properties. We suggest that determining these empirical parameters using both physical and numerical experimentation may provide a more relevant estimate than those provided by the *APS standards* and those cited by others (Pacek et al, 1998; Potten and Wright, 2014). In fact, the work of Pecek et al (1998) is based on a batch stirred vessel with no continuous flow, whose break up mechanism is quite distinct from LJICF under continuous dispersion (Bolszo et al, 2014). The maximum droplet size (d_{max}) and hence the D_{32} values may not be similar for equal amount of energy inputs either. To that end, experimental results of d_{max} for dilute dispersed phase flows are shown to agree well (Simmons and Azzopardi, 2001) with those predicted by Hinze (1955). However, for the case of dense dispersed phase flows, there is a disagreement on the values of d_{max} predicted by the widely used model of Brauner (2004). This only necessitates for more systematic, detailed and synergistic investigation to provide better understanding that can be utilised in a wider area of applications and industries. This important area of investigation will be carried out in our LMPFL using a combination of high speed imaging camera, dual modality Electrical Capacitance Tomography (ECT) and wire mesh tomography (WMT).

2 Synergistic physical and numerical experimentation

As part of a wide range of research and development programme, four experimental and calibration facilities are developed to conduct investigations in the general area of multiphase flows in a synergistic manner. These facilities are depicted by Figure 1.

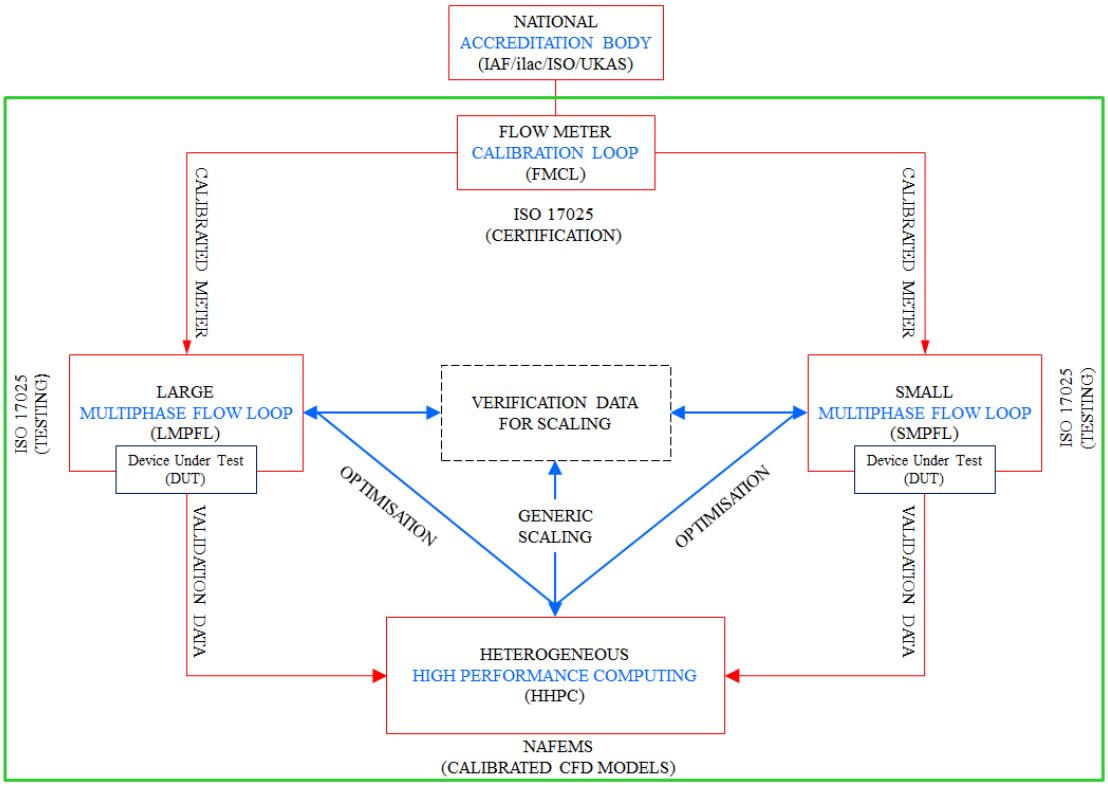

Figure-1: OGH's integrated multiphase flow and computational facility with the aim to understand, predict, verify, quantify and control the evolution of multiphase flows.

The first facility is a small multiphase flow loop (SMPFL) with nominal diameter of 2.5" and with a straight flow stabilisation horizontal section of 25-diameter long, primarily designed to fit in Cambridge University's Magnetic Resonance Imaging unit. The second is a large multiphase flow loop (LMPFL), which is a 4-times scaled up version of the SMPFL both geometrically and dynamically. It has a nominal diameter of 10" and a straight flow stabilisation horizontal section in excess of 100-diameter long. The larger loop has a capacity of up to 350 m^3/hr flow with 10% water. The third facility is a liquid Flow Meter Calibration Loop (FMCL) with a nominal diameter of 12" and with 4" and 8" HTM Master Meter calibration stations to calibrate flow meters of various sizes. It has a flow capacity of 15-600 m^3/hr. Both the SMPFL and LMPFL fall under the calibration and verification audit of the integrated facility. The fourth facility is a Heterogeneous High Performance Computing (HHPC) facility to conduct and validate numerical experiments for any flow of interest and thereby utilise the competence in the optimisation and validation of various multiphase technologies. The system uses the latest and innovative NVIDIA GPU computational hardware heterogeneously coupled with Sandy Bridge CPU cores delivering both high power efficiency and a sustained aggregate performance of 32 "Teraflops". The facility's capacity, accuracy and results from various representative applications will be published elsewhere.

The central theme of these facilities is the quality audit of the practices and procedures by a national accreditation body such as UKAS according to ISO 17025 so that instruments and computer codes are calibrated and certified. A well-controlled and audited experimental data set will provide not only a knowledge pool that can be shared with similar facilities and research centres but also to serve as a testing hub for device manufacturers worldwide with significant benefit for end users too. It will also act as a catalyst for an open forum where a more robust data- or evidence-based prediction, verification, quantification and control of multiphase flows can be made to improve the efficiency and effectiveness of our industry. In this paper, we focus on the use and capabilities of the SMPFL and the HHPC.

2.1 SMPFL construction and operation

The construction and operation of the SMPFL is described in detail elsewhere (Lakshmanan et al, 2015). However, for completeness, we will provide the salient feature of the facility. The loop was constructed so that any device under test (DUT) could be studied with a view to characterise its behaviour and optimise its performance. The DUT is a replaceable unit that permits the characterisation of multiple designs. The nozzles are used to inject a fluid and produce homogeneous flow.

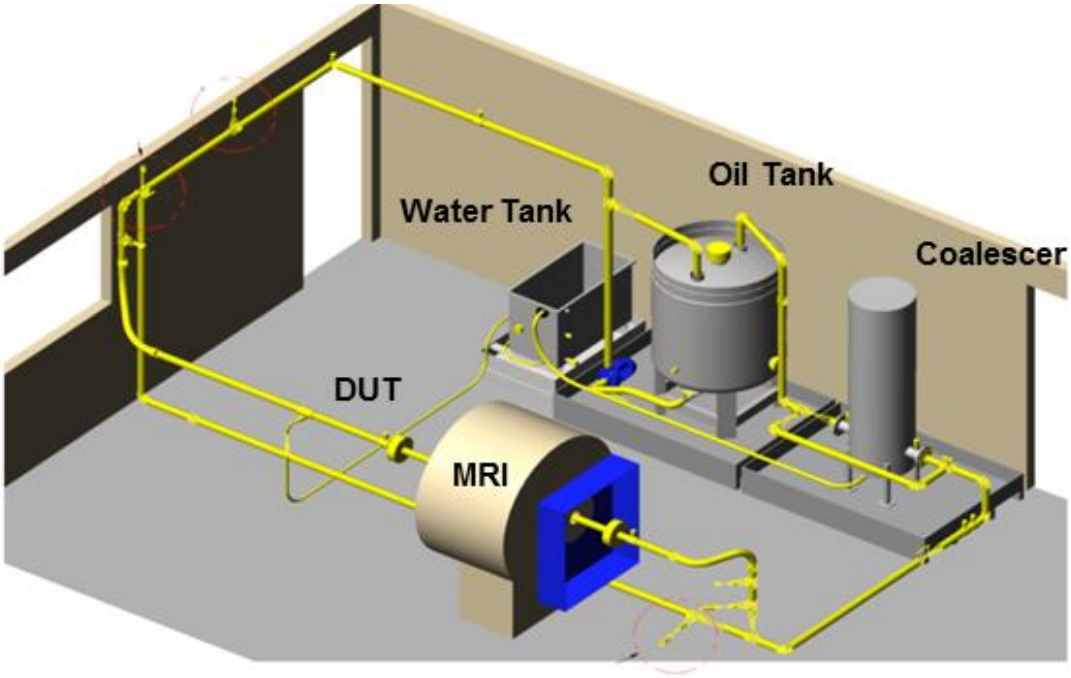

Figure 2: Schematics for the layout of the small multiphase flow loop (SMPFL) as it is fit within Cambridge University's MRI laboratory.

The SMPFL will be used to study the mixing behaviour and efficiency of a prototype homogeniser for liquid sampling in custody transfer applications. The entire SMPFL is designed to be compatible with MR instruments. As such, all piping is manufactured from Durapipe HTA® C-PVC pipework, with the exception of the section where the Zanker plate is positioned and water is injected in to the main oil flow. The layout of the SMPFL and associated MR instrumentation is shown in Figure 2. The section of piping that runs through

the bore of the magnet is constructed from 2.5" diameter schedule 40 clear PVC tubing. The SMPFL is approximately 6 m in length and 3.5 m in width. The 3.5 m width is required to enable the pumps, tanks and coalescer to be positioned outside the 50 G line for the stray field of the magnet. The safety and operability of the flow loop was analysed using HAZOP prior to commissioning. The modules of the SMPFL are:

Coalescer and Holding Tanks Module: The coalescer separates the oil-water mixture and delivers each pure fluid in their respective tanks, where it will be pumped and fed back to the main line to mix again at the flow conditioning and water injection module. The oil and water leaving the coalescer each contains 50 ppm or less of the water and oil phases, respectively. Rustlick EDM-250 oil and de-mineralised water are used. The oil has a specific gravity of 0.81 and viscosity of 2.7 cSt at 40°C. The experiment is carried out within ±2 °C throughout the flow loop.

Flow Conditioning and Water Injection Module: The oil is fed to the loop line via a pump and joins a 2.5" line, where it passes through stainless steel (SST) pipe that contains a Zanker plate designed according to ISO 5167 to ensure flow uniformity and elimination of swirl. Water is then injected 10 pipe diameters (10D) downstream of the Zanker plate in the same direction as the oil flow but at an angle of 23° from the bottom of the pipe so that the desired stream velocities could be achieved for water cut between 0.5% and 5%.

Dynamically Equilibrating Flow (Straight Pipe) Module: This is one of the key modules where the flow is expected to achieve a fully developed multiphase flow to mimic pipeline conditions. However, the length of the straight line pipe was restricted to 25D by the geometry of the MR laboratory in which the experiments are to be performed. As such, extensive baseline tests are carried out to quantify these limitations.

Semi-Automatic Control and Data Capture Module: The loop is operated using a control panel driven by a programmable logic controller (PLC) and data is managed using in-house developed human-machine interface (HMI). All instrument data transmitters capture at a rate of 5Hz except for the temperature transmitters that have a data capture rate of 0.5 Hz.

Homogeniser Module or DUT:: This module consists of a prototype homogeniser device developed by our partners based on a LJICF configuration, where the creation of a horse-shoe turbulent vortex structure provides an exceptionally efficient mixing (Mahesh; 2012). The DUT consists of the nozzle assemblage, the scoop assemblage and a pump as well as pressure, temperature, and flow transmitters. It has also an oil-water mixture sampling point to physically withdraw a sample of known volume to measure its homogeneity.

In the initial experiment without MR, a volume of ~10 mL of the mixture is poured into a graduated flask every other minute in a 10 minute single trial window. For each trial a volume of ~100 ml is captured to verify whether the mixing created by the nozzle is representative as it is withdrawn by the scoop. The scoop take-off that is positioned within 0.1D of the pipe centre is designed to have a take-off area to achieve a nearly isokinetic flow with the pipe stream as stipulated by the *APS standards*. Of course, the wall effect on laminar flow velocity at 0.4D makes it almost a third to that at 0.1D. That is not the case for turbulent flow. The suggestion for the position of the scoop to be within 0.1D, we argue, must has to do with avoiding droplet crossing trajectories, coalescence and fast stratifications.

2.2 Magnetic resonance technique

MR experiments were carried out on a Bruker Biospec (Horizontal Bore) AV spectrometer operating at a 1H frequency of 85 MHz. The spectrometer was equipped with a three-axis shielded gradient coil capable of producing a maximum gradient strength of 10 G cm^{-1} in each direction. An 88 mm diameter radiofrequency coil was used to excite and detect the signal from the fluid. A brief description on the MR technique used in this work is given here, a background on general MR is found elsewhere (Callaghan 1991; Nishimura 2010).

A chemical shift selective (CHESS) imaging sequence was adapted to selectively image the water signal (Haase et al. 1985). In the CHESS method, the radiofrequency pulses are designed to selectively excite the signal from the water whilst suppressing the signal from the oil phase. The pulse sequence for the CHESS excitation used in this work is shown in Figure 3. A 3000 μs Gaussian pulse was used to saturate the signal from the oil. The duration and shape of this pulse is such that a Gaussian distribution of frequencies with a full width at half maximum of approximately 6 ppm is excited. This first pulse acts to saturate both the oil and water signals. Immediately following excitation of the oil peak, crusher gradients are applied in all three directions at a strength of 4 G cm^{-1} to eliminate the signal from (i.e. fully dephase) any magnetisation arising from the oil excitation. The cycle of oil excitation and saturation was repeated four times with the duration of the crusher gradient varied between 3 ms and 5 ms for each cycle. A 7000 μs Gaussian pulse was then used to excite the signal from the water. This pulse will excite a frequency window approximately 2.5 ppm across that is centred upfield of the water peak by 2 ppm. Therefore, this pulse will selectively excite the signal from the water and hence the oil will not be detected. A third, 512 μs Gaussian pulse was used in conjunction with a gradient in the magnetic field to ensure that signal is only detected from a slice of fluid 2 mm thick. This experiment provides a quantitative measurement of the amount of water in the excited volume.

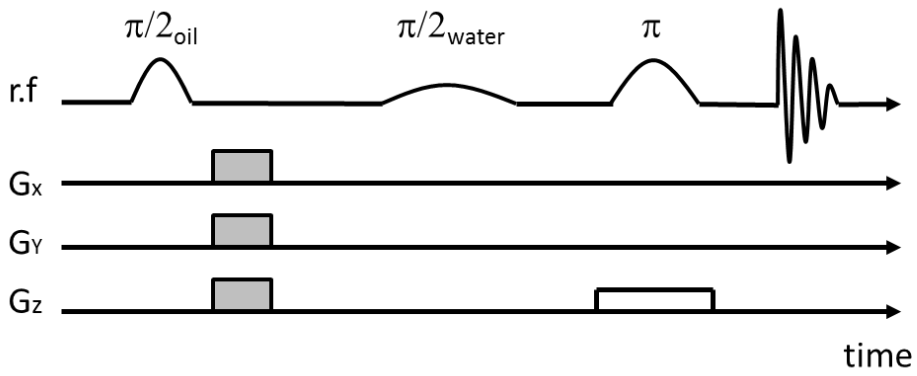

Figure 3: Pulse sequence diagram for the CHESS sequence used for selective imaging of the water in oil-water mixtures. Shaded boxes indicate homospoil gradients; radiofrequency pulses are labelled according to the tip angle and species affected by the pulse. Imaging gradients are not shown, but when these are used they were placed either side of the third, slice selective radiofrequency excitation.

The magnetic susceptibility of oil and water are different and this difference can result in inhomogeneity in the magnetic field. Inhomogeneity in the magnetic field can affect quantification of the water signal. To minimise the inhomogeneity 1.5 mM gadolium

chloride was added to the water. At this concentration, gadolinium does not influence the apparent surface tension of the water phase (Tayler et al. 2011). The addition of gadolinium also has the effect of reducing the T_1 relaxation time of the water to approximately 60 ms, which reduces the time required between measurements and enables quantitative observation of fluid at higher velocity. Furthermore, the short relaxation time of the water will enhance the ability of the CHESS sequence to selectively detect the water signal, in preference to the oil which has a longer relaxation time. The CHESS method was also combined with one- and two-dimensional imaging sequences to resolve the distribution of water spatially. The distribution of water was imaged with a field of view of 193 mm (× 193 mm) and a spatial resolution of 1.5 mm (× 1.5 mm). Oil-water mixtures were prepared with water cuts of 2.5%, 5%, 10% and 25% and measured using each of the pulse sequences in a static phantom. Subsequently, both static and flowing experiments were performed using SMPFL in the absence of mixing, or under well-mixed conditions for water cuts of up to 5%.

2.3 Computational Fluid Dynamics Simulations

Computational Fluid Dynamics (CFD) proves to be a useful design tool to understand the mechanistic behaviour of processes and hence to optimise the efficiency of products. If properly verified and validated, it is also highly cost effective and reliable tool. For example, Boeing's A L Velcci stated with regard to the design of the Boeing 787: "…wind tunnel tests were not used directly for design, but it only helped to verify the accuracy of the computational tools that are used directly to design the aircraft" (Bushnell, 2006). This statement is a testament to the credible use of CFD as a design tool. However, to gain reliable information from such models, validation is crucial. To that end, we set up CFD simulations for the device under test (DUT) as depicted by Figure 4. To verify and also in the future to quantitatively validate our work, the *interFOAM* code in the OpenFOAM® computational framework was adapted and modified to conduct numerical experiments to simulate the LJICF behaviour of the DUT. The modified *interFOAM* code is based on the volume of fluid (VOF) approach (Hirt and Nichols, 1981), which is a modelling technique where the free surfaces of immiscible fluids are tracked so that the phase distribution could be predicted. It does so by solving the phase-fraction transport equation and a single momentum equation for both the phases present.

Interface tracking techniques prove to have unique capabilities to capture liquid jet break up accurately but at a high computational cost. Quantifying the resulting droplet size and its distribution is however still an active area of research which we will address in the future. To obtain a quantitative phase distribution, the phase fraction and momentum equations are solved together with both the standard Reynolds Averaged Navier-Stokes (RANS) and the Large Eddy Simulation (LES) turbulence models. Preliminary tests show that all the RANS based turbulence models were not capable of capturing the mixing characteristics of a LJICF configuration while the LES provided excellent results. However, this was possible after significant modification and implementation of new models as discussed in Lakshmanan et al (2015). Because, like some of the leading VOF based commercial codes (Danielson & Bansal 2012; Desamala et al. 2014), the standard *interFOAM* package was unable to simulate an oil-water flow in a pipe with 50% water cut that exhibits phase inversion. One of the key challenges in the VOF formulation for two phase flow is to preserve the sharpness of the interface between the oil and water phases (Drew & Passman 1998). In most VOF methods,

this issue is handled by a sub-grid level reconstruction using linear or quadratic polynomials (Renardy & Renardy 2002; Diwakar et al. 2009). Our OpenFOAM implementation takes a different route by modifying the advection term for the phase fraction (or water cut) itself. The model is solved using an LES turbulence model using a dynamically-computed eddy-viscosity coefficient for the dynamic Smagorinsky model. Full details of the modified VOF approach will be described elsewhere. The modified VOF model is solved on the mesh shown in Figure 4. The model is applied only to one variant of the nozzle (N1a) while the physical experiments considered four nozzle variants – namely, N1a, N1b, N2a and N3a. While each "Ni"-nozzle serious represent a family of nozzles, the a and b identification represents a variant with the type or family of nozzles (see Table 1).

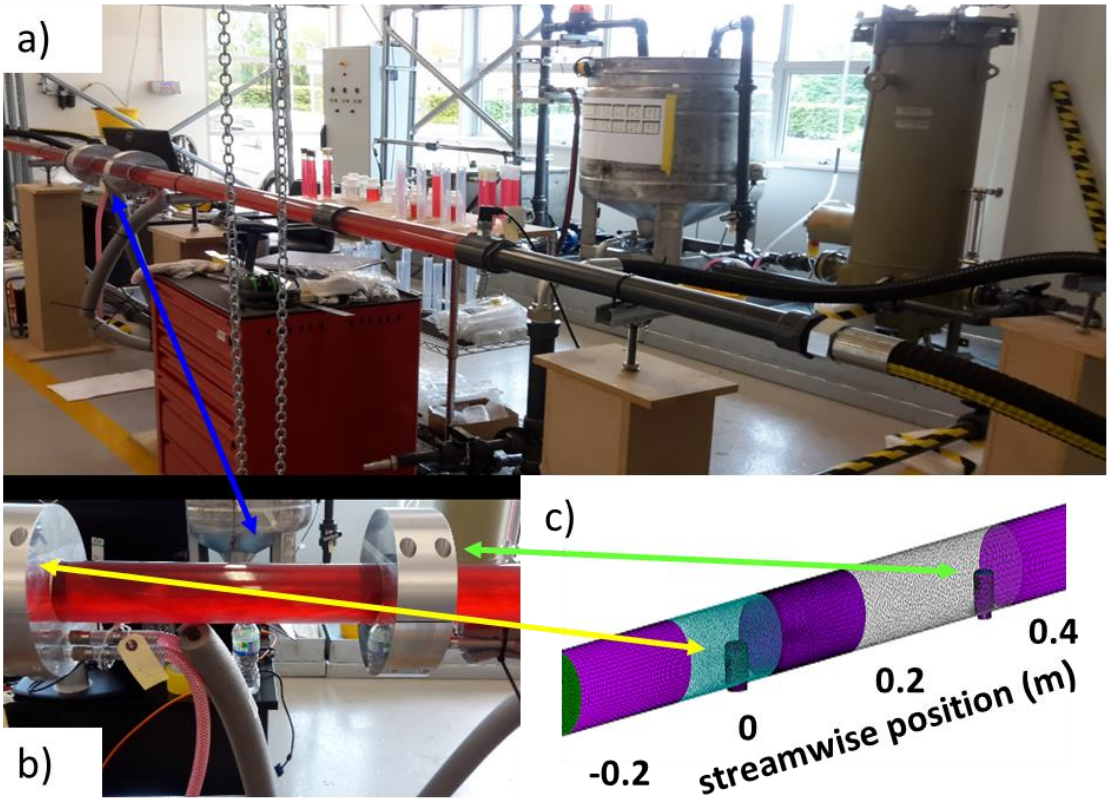

Figure 4: (a) photograph of the Small Multiphase Flow Loop (SMPFL), (b) close up of the homogeniser or device under test (DUT) section, (c) CFD mesh for the DUT showing the nozzle (upstream – x=0m) and scoop (downstream – x~0.4m) positions.

3 Results and discussion

3.1 Design of experiments

The experimental campaign involves three routes or stages. For the SMPFL, two campaigns were carried out where the first involves a physical experiment without MR measurements while the second involves MR measurements both on a phantom of static samples but also with the DUT under static and flowing conditions. When the experiment didn't involve MR measurement, a liquid oil-water sample was withdrawn from the mixed flow instead so that the mixing efficiency can be evaluated. As described by Lakshmanan et al (2015), 16

experiments were conducted using Taguchi's design of experiment. While various parameters were investigated, we would like to note that only one type of nozzle (N1) is used in experimental campaigns 1 and 3. . In the second experimental campaign MR measurement was carried out and two more nozzles types were utilised (N2, N3). Note that the third campaign was a numerical experiment and only N1 was investigated with further optimisation numerical experiments being conducted currently on all types of nozzles. We provide the typical range of operating conditions in Table 1.

	Exp. Campaign 1 (No MR)	Exp. Campaign 2 (With MR)	Exp. Campaign 3 (Numerical)
Nozzle Type (-)	**N1**	**N2, N3**	**N1**
Range of Nozzle-Scoop distance ratio (or **N-S)** (-)	**0.63,1.0**	**0.66, 0.87, 1 (B1, B2, B3)**	**N/a**
Water Cut (%)	**1, 2, 3, 5**	**0, 1, 2, 4, 6**	**2**
Stream Velocity (m/s)	**0.25, 0.5, 0.75, 1.25, 1.5**	**0.2, 0.8, 1.2 (Q1,Q2,Q3)**	**0.5, 1.5**
Range of percent Injected flow rate ratio (or **QJ)** (-)	**0.1, 0.3, 0.5, 1.0**	**0.3, 0.4, 1.0 (QJ1,QJ2,QJ3)**	**1.0**

Table 1: Ranges of parametric and dimensionless values used during the three experimental campaigns. N-S distance is based on normalised values from the nozzle centre (B1, B2, B3). Ranges of QJ is normalised based on its floor and ceiling values.

3.2 Experiment using the SMPFL without MRI

Initially, the SMPFL is used to study the mixing of a standard nozzle that was designed with two variants. The two variants are expected to provide different degree of entrainment atomisation. Therefore, the purpose of the initial experiment is to test the entrainment efficiency of the nozzles so that only a selected few nozzles will be used for the MRI experiments at a later stage of the development. The design of experiment (DoE) for this initial stage of work used the Taguchi technique and 16 experiments were conducted with three trials in each as reported by Lakshmanan et al (2015). Depending on the variations of the chosen factors, the 16 experiments were conducted in 4 groups. Figure 5 shows a summary of the accuracy of the water cut for these experiments. These measurements were obtained by sampling the oil-water mixture that was withdrawn through the scoop, as illustrated in Figures 2 and 4. The oil-water samples were allowed to settle for two more days before the water fraction was measured. No permanent emulsification is observed on these samples. The samples in the graduated cylinder were measured for total liquid height and water height using a TOMARCH PN 31761 digital height gauge with measurement accuracy of 0.0127 mm. The water cut was calculated by dividing the water volume by the total volume of liquid. Measurements by three operators were taken and checked for repeatability. Similarly, each of the three experiments captured via the HMI were checked for repeatability.

The measured fraction of water obtained from the scoop is compared with the known fraction of water based on the measured oil and water flow rates. A relative accuracy was established and the results are shown in Figure 5. Except for three data points, the mixing achieved falls within the requirements of the *APS standards*. The results demonstrate a complex behaviour

on the degree of mixing that can be achieved. Although the *APS standards* stipulate that for a horizontal pipe with stream velocity in excess of 2.4 m-s^{-1} adequate natural mixing may be achieved, our results indicate that this is not the case. Furthermore, the *APS standards* recommend the scoop take off velocity to be isokinetic and, for a horizontal pipe, the scoop inlet area is depicted by a figure to be placed within 0.1D below its centre, which will only allow 1% injection for a circular inlet. Of course, the *APS standards* indicate wall effect to be of consideration. But, velocity profile encompasses the wall effect and at that location it is likely to provide best option to avoid droplet crossing trajectories so that a more representative sample is withdrawn. In addition, our results indicate that an injection of 5% is often required. In fact, injecting 1.8% of the total flow rate with stream velocity of 1.47 m/s proved to provide the worst mixing. For a weak jet with 1.8% injection, the stream momentum flux is overwhelming and hence the jet collapses without providing sufficient mixing. This indicates a limitation on *APS standards* both in their specification or the manner it could be interpreted. More importantly, how mixed-ness is quantified. However, for a stratified flow with stream velocity less than 0.75m/s and with an injection of 8% of the total flow rate, it is possible to achieve homogeneous mixing in a horizontal pipe that satisfies the minimum requirements of the *APS standards*. Indeed the results indicate that the extent of mixing is dependent primarily on the velocity and momentum flux ratios, and is not very sensitive to the water cut, which was not expected. However, eq. (1) suggests that the mixing will be a strong function of water-cut if the water cut becomes high or the stream velocity is too low and the resulting entrainment atomisation creates a dense dispersed phase that may result in collision and coalescence of water droplets thereby enhancing stratification.

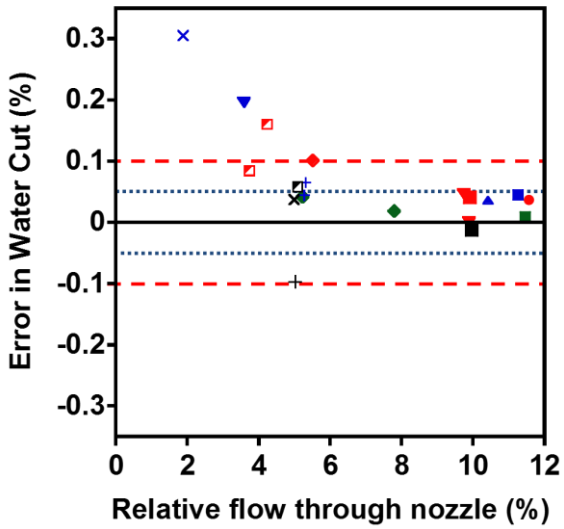

Figure 5: Plot of the relative error of water cut as a function of the injected flow into the mixing nozzles grouped by velocity (identified by symbols) and water cut (identified by colour). The symbols indicate water cut (black) ~1%; (red) ~2%; (blue) ~3%; and (green) 3.5% and stream velocities (●) ~0.25 m/s; (▲) 0.35 m/s; (■) ~0.43m/s; (♦) ~0.54m/s; (▼) ~0.77m/s; (+) ~0.81 m/s; (◩) ~1.15 m/s and (×) ~1.47 m/s. The x-axis shows the injected flow rate relative to the total oil-water flow rate through the pipe. The red dashed lines indicate a level of better than 90% mixing as required by the *APS standards*. However, the blue dotted lines indicate a level of 5% mixing, which is twice better than the minimum requirement. The mixing also appears less sensitive to the water cut, which is unexpected.

The results obtained using the SMPFL demonstrate that there is a need for a better understanding of the homogenisation process when using the LJICF arrangement. In the next sections, we present the numerical- and physical-experiment results that enabled us to study the homogenisation process in more detail than has hitherto been possible.

3.3 Numerical experiment using the HHPC facility

CFD simulations were carried out on the LJICF configuration for an initially stratified oil-water flow for a range of nozzle orientations, fluid velocities and spacing of the scoop. Figure 6 gives a summary of the results of one of these simulations. Figure 6(a) shows the instantaneous speed (magnitude of the velocity) of the fluid in the pipe. High speeds are observed in the vicinity of the jets of the nozzle, as expected. These high speed liquid flows enhance the jet-break up and generate the turbulence and mixing that is used to homogenise the distribution of water throughout the cross section of the pipe.

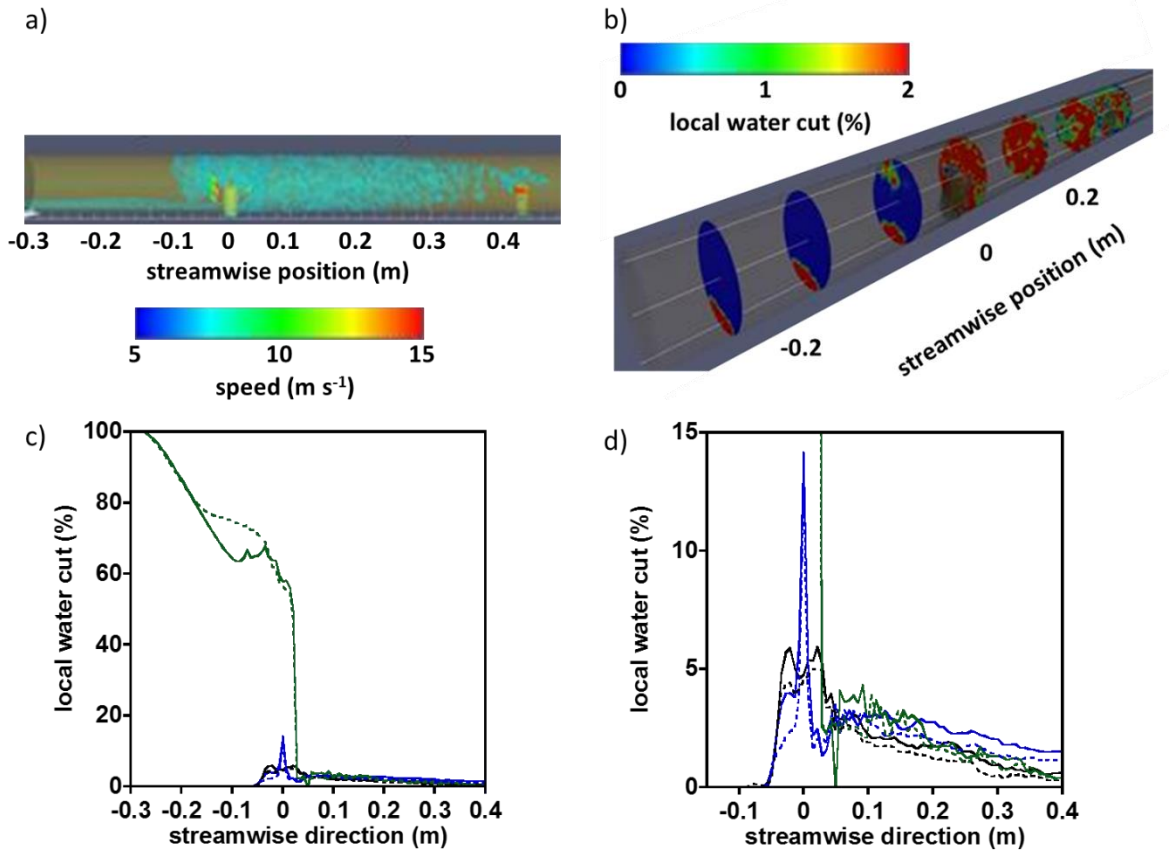

Figure 6: Example results from the CFD simulations showing (a) speed of the liquid in the homogenization section (DUT), (b) maps of the local water cut at different positions along the length of the pipe, (c) plot of the water cut at the top (black), middle (blue) and bottom (green) of the pipe for overall water cuts of 2.0% with stream velocities of 0.5 m s-1 (dashed lines) and 1.5 m s-1 (solid lines). (d) shows the same data as in (c), but with the vertical scale reduced to highlight differences in the local water cut.

Figure 6(b) illustrates the improvement in the homogenization that is achieved downstream of the nozzle for the simulation conditions shown in Figure 6(a). Upstream of the nozzle injection, the flow is stratified with water only visible in a narrow channel along the base of

the pipe. As soon as the flow approaches the nozzle, the water is rapidly distributed across the cross section of the pipe. Downstream of the nozzle the flow becomes increasingly homogeneous. To quantify the distribution of water and compare this simulation with the industry standard criteria, the mean water-cut averaged over time as well as over the immediate neighbouring computational cells is shown in Figure 6(c). The local water cut is shown at the top, bottom and in the middle of the pipe for stream velocities of 0.5 m s-1 and 1.5 m s-1. Initially the flow is fully stratified and so the local water cut taken from the middle and top of the pipe show no water, and as expected, the local water cut at the bottom of the pipe is 100%. The nozzle is defined as the origin of the coordinate system and at this point the water cut at the bottom of the pipe rapidly decreases, whilst the water cuts in the middle and at the top of the pipe increase. Figure 6(d) shows the same data as Figure 6(c), but with a finer scale such that it is possible to resolve the differences in the water cut at the different heights in the pipe. Downstream of the nozzle, the average water cut in the middle of the pipe, for both the 0.5 m s-1 (dashed lines) and 1.5 m s-1 (solid lines) stream velocities is close to the 2% water cut that is expected for a homogenously mixed flow in this case, but significantly greater than those at the top or bottom of the pipe. However, both the top and bottom water cut values are less than those in the middle which means that the water is sufficiently lifted from the bottom wall, which is key. Overall the stratified water is now fairly evenly distributed as manifested by the overlapping graphs at 2% water cut values in Figure 6(d), satisfying the *APS standards*. Further simulations (not shown) indicate that the flow rate through the nozzle has a strong effect on the homogenization process. This result is consistent with the experiments performed on the SMPFL during experimental campaign 1.

3.4 MR Measurements of static samples

Four different commercial oils (Rustlick EDM-250, VG 5, kerosene, and SAE 30) with viscosities between 3 cSt and 100 cSt were tested using MR. Rustlick EDM-250 and VG 5 both have a high flash point and low viscosity making them a suitable model at low temperature for oil-water experiments and safe to use.

The spectrum of mixtures of oil and water for all four oils were similar, with the resonance of the oil peak appearing at a chemical shift approximately 4.5 ppm lower than the water peak in all cases. These oils are therefore essentially equivalent from the perspective of MR. At this point it is worth noting that the imaging spectrometer used for these experiments does not provide the homogeneity or stability of the magnetic field that are required for high resolution spectroscopic measurements; therefore the detailed chemical structure of the oil species is not visible in the spectra. Static oil-water mixtures were prepared with water-cuts between 2.5% and 25%. Figure 7(a) shows the magnetic resonance spectrum following CHESS excitation of two samples. The water peak is located at 5.5 ppm, whilst the oil peak would be located at 1 ppm. The oil peak is almost completely suppressed, meaning that the amount of water is calculated easily by integrating the signal intensity from the remaining peak. The integral of the signal between 5 and 6 ppm, which is attributed to the water, is calculated and plotted against the known water cut, as shown in Figure 7(b). Each experiment was repeated between two and five times at different positions within the same static sample to provide an indication of the reproducibility of the experiments. Error bars, given by the 95% confidence interval, are shown in Figure 8 for both the measured signal intensity and the water cut. The error bars are mostly comparable in length to the size of the symbols in the plot and so are

difficult to resolve. A larger error is observed for the water cut of 10% which is attributed to a poor shim for this sample. The total signal intensity associated with each measurement had a standard deviation of about 0.1 (a.u.) for each water cut. The integrated signal intensity shows a linear relationship with the water cut. A linear fit through these data yields a slope of 0.385 ± 0.005%$^{-1}$ with an R^2 value of 0.999. These results demonstrate that MR provides quantitative measurements of the water cut. On the basis of the calculated slope, an uncertainty in the signal intensity of 0.1 corresponds to an error in the measured water cut of approximately 0.2%, even for the poorest quality measurements obtained with the 10% water cut the uncertainty of the water cut is less than 1%.

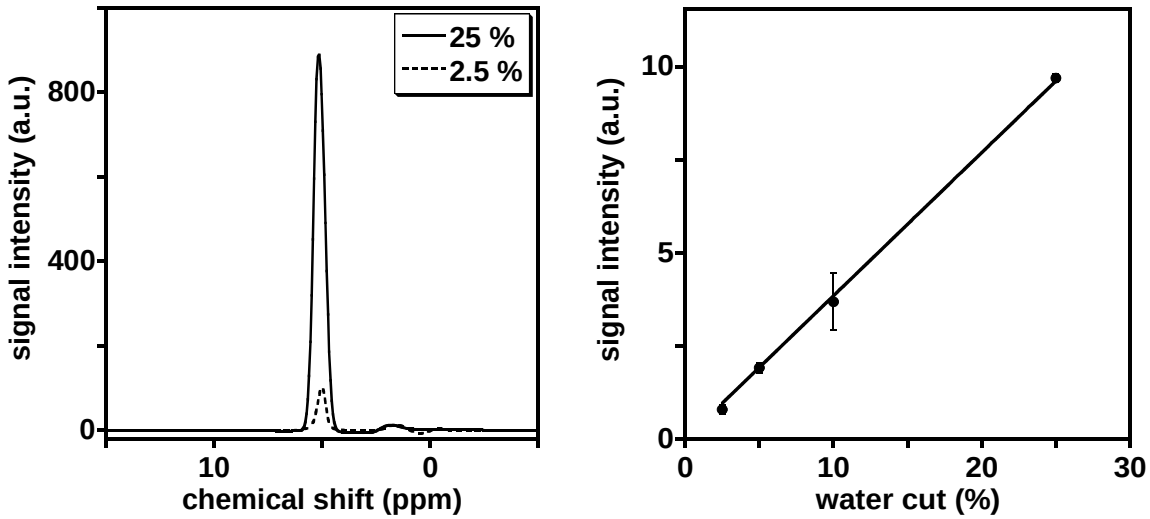

Figure 7. (a) MR spectra obtained from water-oil mixtures at 2.5% and 25% water. Spectra were obtained using the CHESS sequence to suppress signal from the oil peak. The water peak is located at approximately 5.5 ppm; the peak arising from the oil is largely suppressed but would be located at approximately 1 ppm. (b) Plot of the integrated signal intensity as a function of the water-cut. The solid line is a linear fit to the data passing through zero. The slope of the line is 0.385 ± 0.005%$^{-1}$

Static oil-water phantoms were prepared with water cuts of between 5% and 25% to demonstrate two-dimensional (2D) MR imaging of water within the pipe. However, ultrafast 2D MR measurements on fast-flowing oil-water mixtures are extremely challenging. Instead here we obtain time-averaged images of the distribution of oil and water. An example of the two-dimensional images that will be obtained of the oil-water flow is shown in Figure 8 for static samples of 10% and 25% oil-water mixtures. In these images, in each case, two distinct layers can be seen; one is almost pure water while the other is almost pure oil. To aid visualisation, the approximate outline of the pipe is sketched on Figure 8 using a dashed white line. The cross section of the pipe that contains water in Figure 8 is clearly visible, and can be calculated to be 3.0 ± 0.3 mm2, and 7.6 ± 0.3 mm2 for the 10% and 25% samples, respectively. The total pipe area is 30 mm2, thus, the measured cross sectional areas are in good agreement with the volume fraction of the samples. The spatial resolution of the images is 1.5 mm × 1.5 mm and the acquisition time was 120 s. The acquisition time could be reduced but for later experiments on flowing systems reducing the acquisition time would have the effect of reducing the apparent signal-to-noise ratio owing to fluctuations arising

from the time varying nature of the flow. The signal intensity is proportional to the water content, as shown in Figure 7(b).

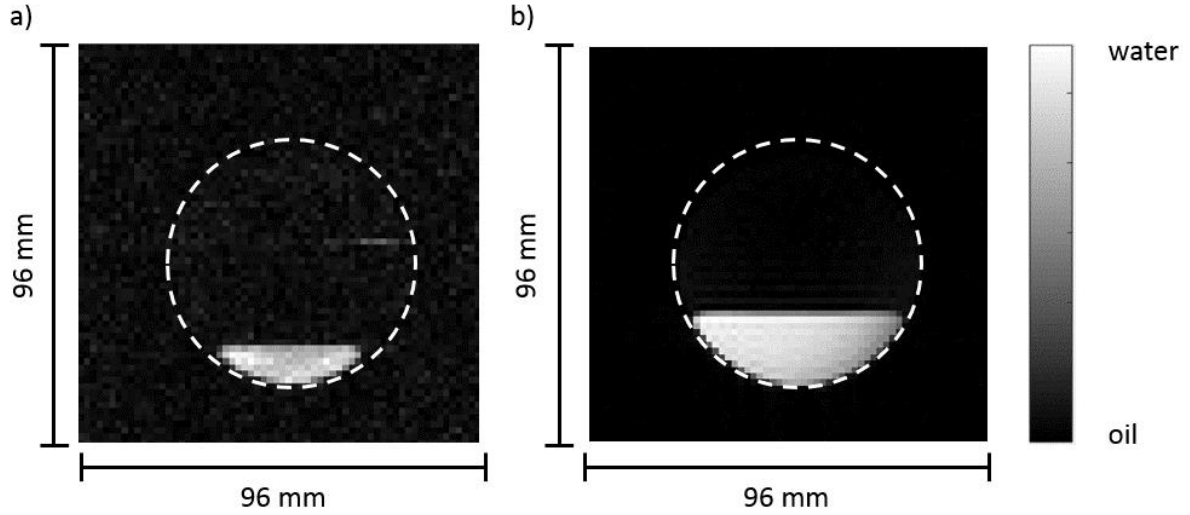

Figure 8. 2D MR images of stratified water cut distribution for a static oil-water system through the cross section of the pipe with (a) 10% and (b) 25% water-cut.

Therefore, these images provide a direct measure of the amount of water at each position within the pipe. The water cut at each location is estimated to be accurate to within ±1%, based on the apparent signal-to-noise ratio of the image. Additional changes in signal intensity of up to 10% arise from variation in the sensitivity of the radiofrequency coil. In the future these variations will be eliminated by using a map of the sensitivity distribution of the coil (Holland et al. 2009). The accuracy of these time-averaged measurements could be further improved by increasing the total acquisition time, provided that the pipe flow is operating in a steady state, which is crucial. The CHESS sequence was then combined with imaging sequences to enable visualisation of the water distribution through the pipe. A stationary system in a horizontal pipe was imaged, where the denser water phase remains on the bottom of the pipe whilst the lighter oil phase fills the top of the pipe. Stratified flows of such type are commonly encountered in the oil and gas sector and represent a worst case scenario from which to achieve a homogeneous mixture.

3.5 MR Measurements during flowing conditions

In order to demonstrate that the MR measurements are quantitative, the signal intensity from the spectral acquisitions was plotted for well mixed flow of oil and water at water cuts between 1% and 6%, as shown in Figure 9. The plot shows a linear correlation, as was seen with the static measurements shown in Figure 7(b). A linear fit through these data gives slopes of $(1.9 \pm 0.1) \times 10^7$ $\%^{-1}$ and $(2.1 \pm 0.1) \times 10^7$ $\%^{-1}$ for stream velocities of 0.8 m s^{-1} and 1.2 m s^{-1}, respectively. The fact that this slope is essentially constant for changing stream velocity indicates that the effects of in-flow are insignificant in this case. The inherent noise level in the data is $\sim 1 \times 10^6$, indicating that the water cut can be measured with an accuracy of approximately ±0.2 % using MRI.

Figure 10 shows 2D MR images of a stratified oil-water flow at water cuts of 2% and 7.5%, based on the flow rate of oil and water in the system. These images are equivalent to those shown in Figure 8, but acquired under flowing conditions such that the oil and water phases are stratified and do not mix. It is clear from these images that the water remains largely confined to the base of the pipe and little water mixes into the bulk oil flow, as expected. It is also interesting to examine the cross sectional area of the pipe filled with water in both cases.

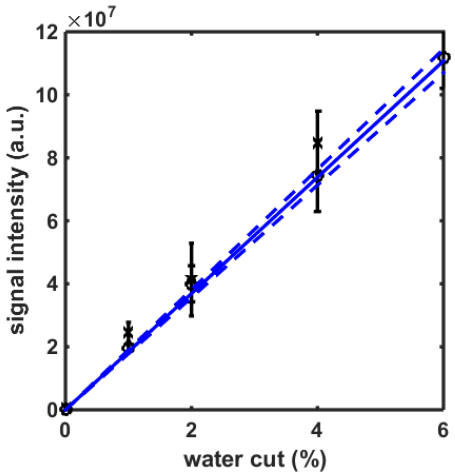

Figure 9. Signal intensity from MR experiments performed on a well-mixed system operating with a stream velocity of the oil phase of (○) 0.8 m s^{-1} and (×) 1.2 m s^{-1} and for water cuts of up to 6% based on the measured volumetric flow rate of oil and water. The solid line indicates a linear fit to the data, with the dashed lines indicating the 95% confidence interval for this fit. The error bars for the measured data points indicate two standard deviations in the measured signal intensity.

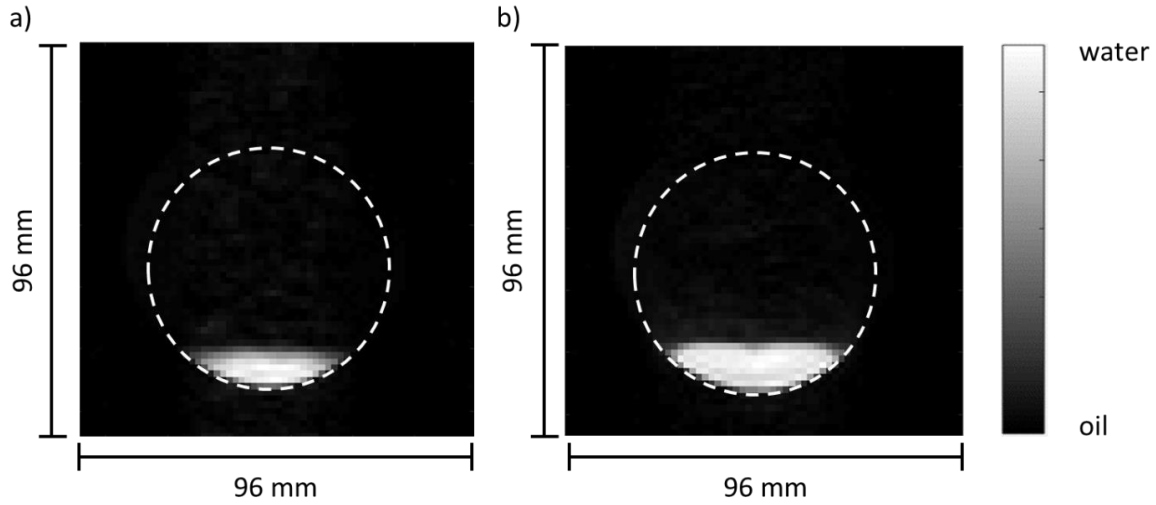

Figure 10. 2D MR images of the distribution of water through the cross section of the pipe during stratified flow with (a) 2% and (b) 7.5% water, based on the measured volumetric flow rate.

The interface between the water and the oil in Figure 10 is no longer characterised by a sharp interface as was seen in Figure 8. This is due to some flow instability at the oil-water interface, even if it is at low velocity. In these time-averaged images, this instability

manifests as a gradual change in water content from pure water to pure oil. In spite of this, it is still possible to estimate the cross sectional area of the pipe that is filled with water. In this case the proportion of the pipe area occupied by the water at nominal water cuts of 2% and 7.5%, is 9 ± 2% and 15 ± 1%, respectively. The uncertainty is calculated on the basis of the sharpness of the interface between the oil and water phases. It is clear that for these experiments, the cross sectional area of the pipe occupied by water does not scale with the water cut measured on the basis of the flow rate of oil and water through the system.

In order to investigate these observations further, 1D profiles were acquired along the height of the pipe, as shown in Figure 11. These plots provide an indication of the amount of water present at each vertical position, integrated across the width of the pipe. Profiles are shown for stream velocities of 0.2 m s^{-1}, 0.8 m s^{-1}, and 1.2 m s^{-1}, with nozzles N2 and N3. For perfect mixing, the curves would be expected to be shaped like a hemi-circle, as this is the projection of the cross section of the pipe (Lakshmanan et al, 2015). It is clear that the profiles do not conform to this ideal shape for any of the results shown. The discrepancy is largely due to the inhomogeneity of the magnetic- and radio-frequency fields used but also the inhomogeneity of the mixing and unsteadiness of the flow. Despite, the profiles only providing a qualitative indication of mixing, some insight into the flow and mixing within the pipe can be gained.

As the water cut increases, it is clear that the fraction of the pipe filled with water increases, as expected. At the very low stream velocity of 0.2 m s^{-1} that is typical of oil fields with end of production expectancy, high signal is obtained from the bottom of the pipe while using nozzle N2, indicating the presence of a relatively high concentration of water along the base of the pipe. However, the amount of water at the base of the pipe is slightly less for N3 than nozzle N2. In both cases, at the very low velocity, full mixed-ness is not achieved.

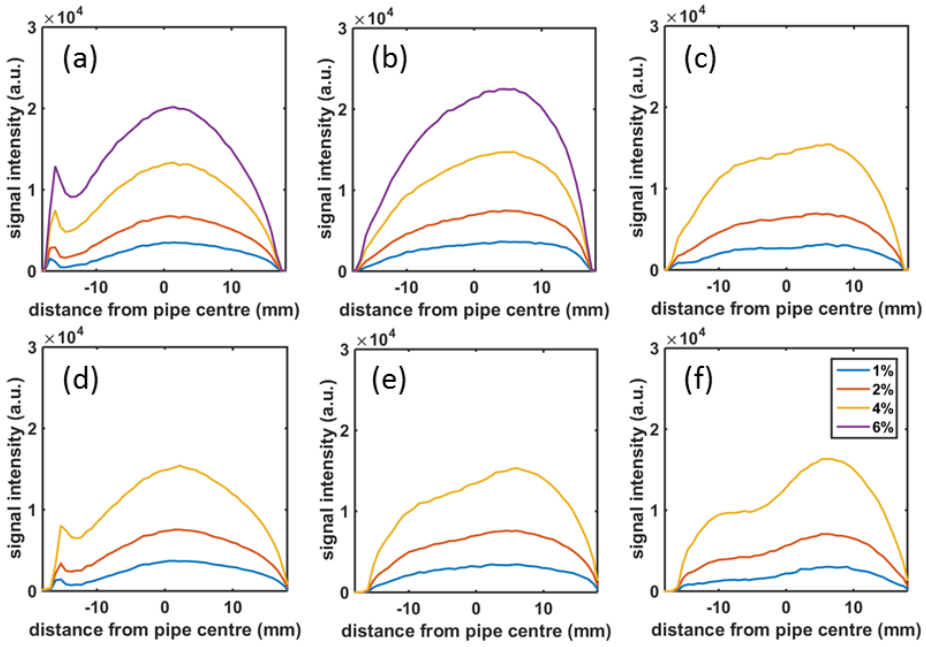

Figure 11. Profiles of the average water distribution in the pipe 330mm downstream of the injection nozzle N2 (a-c) and nozzle N3 (d-f). The stream velocities are (a, d) 0.2 m s^{-1}, (b, e) 0.8 m s^{-1} and (c, f) 1.2 m s^{-1}.

It is instructive however to observe that the minimum requirement for homogeneous mixing could be met by using the so called C1/C2 ratio in the *APS standards*, which is obtained by taking samples above and below the centre-line of the pipe at say 0.5 × R, where R is the radius of the pipe. The profile is approximately symmetric for up to 2/3rd of the pipe radius, therefore the C1/C2 ratio will be close to one. However, what is demonstrated here is that the C1/C2 ratio is not a good measure of mixed-ness as it does not account for the stratification of the flow seen here. At higher stream velocities, the distribution is more homogeneous and for both nozzles, the distribution of water is essentially the same at stream velocities of 0.8 m s^{-1} and 1.2 m s^{-1}. The similarity in the shape of the profiles for a variety of water cuts and stream velocities indicates that the water is likely well mixed in these cases.

To elucidate the mixing further, a quantitative water-cut profile was obtained by dividing the profiles from Figure 11 by the profile of a static oil sample, as shown in Figure 12. This normalisation of the signal by the signal from a static oil sample helps correct for variations in the signal intensity arising from inhomogeneity in the radiofrequency and magnetic fields used in these experiments. The remaining signal can then be correlated with the known total water cut, as in Figure 9, to provide an estimate of the local water cut. At a velocity of 0.2 m s^{-1} the normalisation is effective as this corresponds to laminar flow and thus the flow is stable over time. In this case, the local water cut is measured with an estimated accuracy of ±0.5%. In the case of turbulent flow, the measurements are not as stable over time and a systematic bias in the measurement is introduced at different locations within the pipe. Thus, for turbulent flow the error is estimated to be approximately ±3%.

Figure 12 is organised to show the parametric dependence and the characterisation of nozzles N2 and N3. For example, row (a,b,c) shows the mixing effectiveness as a function of stream velocity and water cut, whilst column (a,d,g) shows the evolution of stratification at different distances downstream from the nozzle injection position. In a perfect mixing condition, the water cut profiles are expected to be flat indicating a constant water cut throughout the pipe. The profiles are significantly flatter than those shown in Figure 11, however some curvature remains. For the turbulent flow profiles, the instability of the flow means that the uncertainty in the measurement is large and the flow may be regarded as being well mixed within the experimental uncertainty (±3% in this case). For the lowest velocity, the flow was laminar and the results are more accurate (±0.5%). The results confirm that stratification is significant for the lowest flow rate and that this increases downstream of the injection point. Using these quantitative measurements of the local water cut, it is possible to estimate the error that would be introduced into a flow measurement that does not sample from the base of the pipe. At a water cut of 1% the error is negligible (about 1.04% vs 1%), however, at a water cut of 6% the error is significant (true water cut about 9% vs 6%) for the worst case condition of the data at position B3 (see Figure 12(g)).

Two dimensional images of the flow were also obtained for a few of these flow conditions. Figure 13 illustrates two of these images, taken from the (a) worst and (b) best mixing scenarios at a water cut of 4%. These experiments correspond to the profiles in Figures 12 (a) and (k)). A bright region is clearly visible at the bottom of the pipe in Figure 13(a), indicating the presence of almost pure water in a thin line around the base of the pipe. By contrast at the higher flow velocity, the image intensity is fairly uniform indicating that the fluid is well mixed.

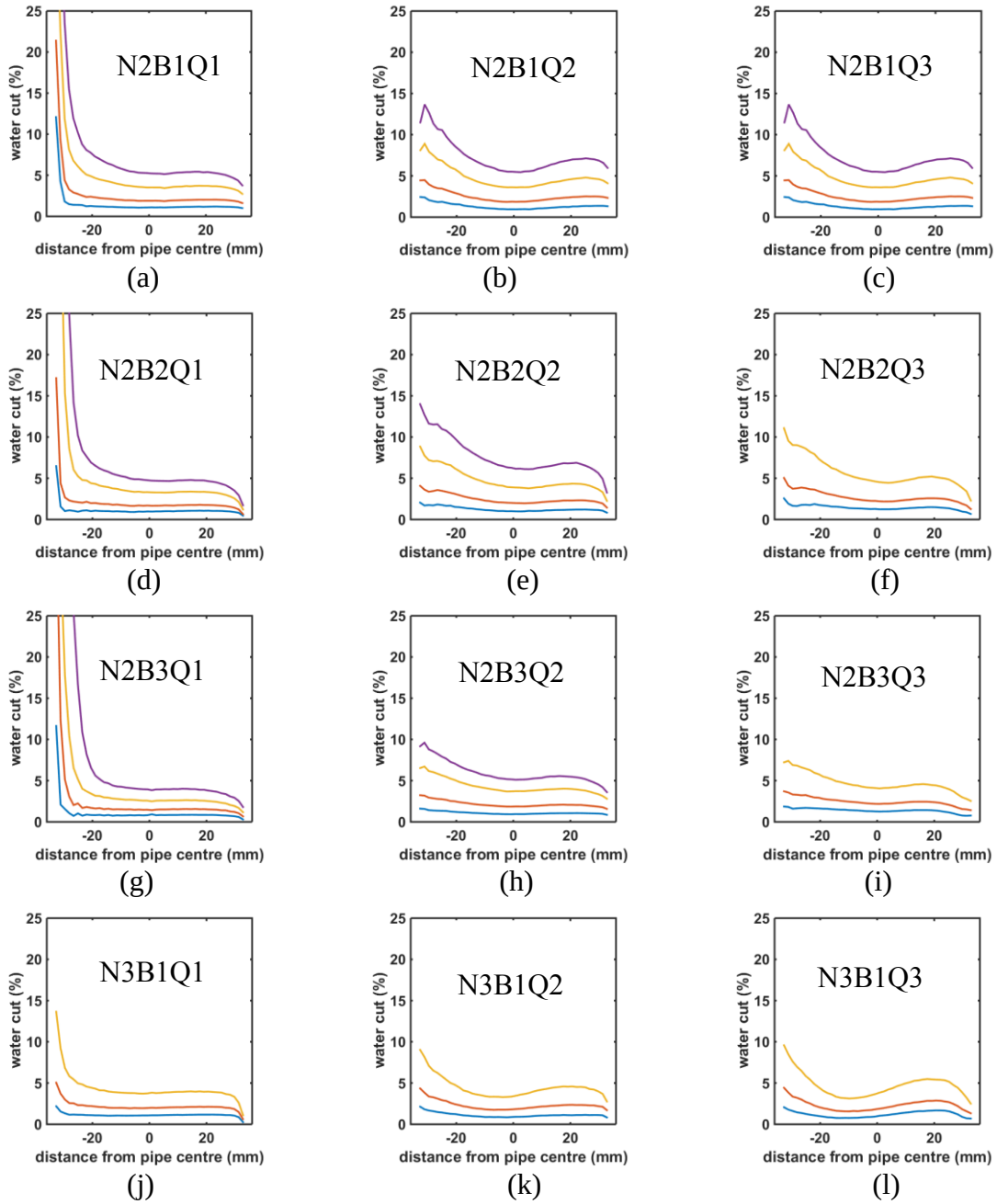

Figure 12. Water cut profiles obtained by normalising the data from Figure 11. (a-i) are for Nozzle Type 2 (N2), whilst (j-l) are for Nozzle Type 3. (a-c) and (j-l) were taken XX downstream of the nozzle, (d-f) were taken YY downstream of the nozzle and (g-i) were acquired ZZ downstream of the nozzle. For all nozzles types, the columns correspond to different stream velocities of 0.2 m s^{-1} (Q1), 0.8 m s^{-1} (Q2), and 1.2 m s^{-1} (Q3). An important comparison between nozzle types N2 and N3 is depicted by rows (a,b,c) and (j,k,l), for the same dynamic condition and "N-S" value B1. (j-l) shows a clear reduction in the quantity of water at the base of the pipe when compared with (a-c), particularly at the most challenging Q1 value. The range of water cut values is shown in colour blue (1%), gold (2%), yellow (4%) and purple (6%). Not all the experiments utilise 6% water cut.

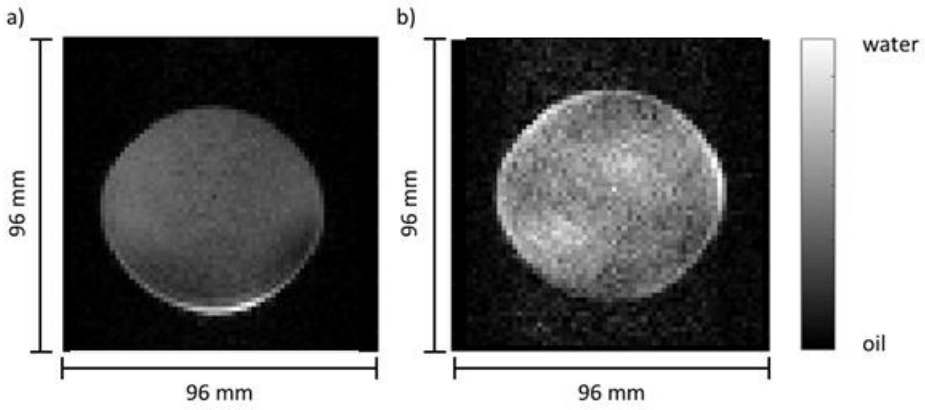

Figure 13. 2D MR images of the distribution of water through the cross section of the pipe during a flowing condition for water cut of 4% with (a) nozzle N2 at stream velocity of 0.2 m s^{-1} (b) nozzle N3 at a stream velocity of 0.8 m s^{-1}., both at N-S distance B1. The bright white region at the base of (a) indicates a high local water fraction, however small it looks.

4 Conclusion

As part of a large research and development work, we have commissioned a small multi-phase flow loop (SMPFL) with a Liquid Jet In Cross Flow (LJICF) configuration to study liquid-liquid flows using computational fluid dynamics (CFD) and magnetic resonance imaging (MRI). First, a numerical simulation technique was developed using the open source computational platform OpenFOAM®, where a modified Large Eddy Simulation (LES) method was utilised to capture the oil-water flow regimes and the resulting mixing behaviour due to a novel homogeniser. This initial simulation allowed optimising the design of the homogeniser that ought to comply with the *APS standards*. Once the homogeniser is manufactured and the SMPFL is operational, MR measurement technique using a CHESS sequence was used to capture the data for different nozzles and mixing operating conditions. The static oil-water composition is quantified to within 0.2%. In addition, by combining the CHESS sequence with imaging, one- and two-dimensional profiles of the water distribution throughout the cross-section of the pipe were obtained. For the case of laminar flow, the accuracy of the water cut is ±0.5% while for turbulent flow case, the accuracy is ±3%, which is within measurement uncertainty. It is important to interrogate the large data set we have to extract the hydrodynamic artefacts that may have likely pronounced some of the water cut values observed. However, these results highlighted various issues related to both the general area of LJICF for liquid-liquid systems but also some unresolved issues in the current APS standards, not only on their interpretation but also on key assumptions. Understanding the mechanisms of Jet break-up, droplet formation and size distribution may hold the key.

5 Acknowledgement

The authors are grateful for the financial support from Innovate UK and the Engineering and Physical Sciences Research Council through grant KTP009424. Technical support has been provided by Dr Mick Mantle, Magnetic Resonance Research Centre (MRRC), University of Cambridge; engineering and operational support was provided by Oil & Gas Holdings. The authors also acknowledge the continuing support from Mr Steve O'Donnell, Chairman of the Innovate UK Local Management Committee (LMC) and MD, Oil & Gas Systems Ltd.

6 References

ANGELI P., HEWITT G.F., (2000), Drop size distributions in horizontal oil-water dispersed flows, *Chemical Engineering Science.*, 55 3133–3143.

API 8.2 (1995). Standard Practice for Automatic Sampling of Liquid Petroleum and Petroleum Products, American Petroleum Institute.

BIEBERLE A., HARTING H., RABHA S., SCHUBERT M., HAMPEL U., (2013), Gamma-Ray Computed Tomography for Imaging of Multiphase Flows. *Chemie Ingenieur Technik.*, 85 1002–1011.

BOLSZO, C. D.; McDONELL, V. G., GOMESZ, G. A., SAMUELSEN, G. S., (2014), Injection of water-in-oil emulsion jets into a subsonic crossflow: An experimental study, *Atomisation and Sprays*, 24(4):303-348.

BRAUNER, N., (2001). The prediction of dispersed flows boundaries in liquid-liquid and gas-liquid systems, *Int. J. Multiphase Flow* 27:885-910.

BUSHNELL DM, (2006). Scaling: Wind Tunnel to Flight, Ann. Rev. Fluid Mechanics, (**38**): 111-128

CALLAGHAN P.T.,(1991), *Principles of nuclear magnetic resonance microscopy*, Oxford: Clarendon Press.

CLARK B.J., (1964), Breakup of a liquid jet in a transverse flow of gas, *NASA TN D.*, 2424.

DANIELSON T.J., BANSAL K.M., (2012), Simulation of Slug Flow in Oil and Gas Pipelines Using a New Transient Simulator. In *Offshore Technology Conference.*, ConocoPhillips.

DESAMALA A.B., DASAMAHAPATRA A.K., MANDAL T.K., (2014), Oil-Water Two-Phase Flow Characteristics in Horizontal Pipeline – A Comprehensive CFD Study. *International Journal of Chemical, Nuclear, Materials and Metallurgical Engineering.*, 8 336–340.

DIWAKAR S. V., DAS, S.K., SUNDARAJAN T., (2009), A Quadratic Spline based Interface (QUASI) reconstruction algorithm for accurate tracking of two-phase flows. *Journal of Computational Physics.*, 228 9107–9130.

DREW D.A., PASSMAN S.L., (1998), *Theory of multicomponent fluids*, New York: Applied Mathematical Sciences., vol 135, Springer-Verlag.

ELKINS C.J., ALLEY M.T., (2007), Magnetic resonance velocimetry: applications of magnetic resonance imaging in the measurement of fluid motion. *Experiments in Fluids.*, 43 823–858.

FERNANDO L.M., LENN C.P., (1990), Jet mixing of water in crude oil pipelines for representative sampling. *Analytica Chimica Acta.*, 238 251–256.

FUKUSHIMA E., (1999), Nuclear magnetic resonance as a tool to study flow. *Annual Review of Fluid Mechanics.*, 31 95 –123.

GALINAT S., MASBERNAT O., GUIRAUD P., DALMAZZONE C., NOIK C., (2005), Drop break-up in turbulent pipe flow downstream of a restriction. *Chemical Engineering Science.*, 60 6511–6528.

GEERY E.L., MARGETTS M.J., (1969), Penetration of a high-velocity gas stream by a water jet. *Journal of Spacecraft and Rockets.*, 6 79–81.

GLADDEN L.F., SEDERMAN A.J.,(2013), Recent advances in Flow MRI. *Journal of Magnetic Resonance.*, 229 2–11.

GOTZ J., ZICK K., (2003), Local velocity and concentration of the single components in water/oil mixtures monitored by means of MRI flow experiments in steady tube flow. *Chem. Eng. and Tech.* 26 59–68.

HAASE A., FRAHM J., HANICKE W., MATTHAEI D., (1985), 1H NMR chemical shift selective (CHESS) imaging. *Physics in medicine and biology.*, 30 341–344.

HAASE A., FRAHM J., MATTHAEI D., HANICKE W., MERBOLDT K.D., (1986), FLASH imaging. Rapid NMR imaging using low flip-angle pulses. *Journal of Magnetic Resonance.*, 67 258–266.

HENNIG J., NAUERTH A., FRIEDBURGH H., (1986), RARE imaging: a fast imaging method for clinical MR. *Magnetic Resonance in Medicine.*, 3 823–833.

HINZE, J., (1955), Fundamentals of the hydrodynamic mechanism of splitting in dispersion processes, AIChE J. 1:289-295

HIRT, C. W., NICHOLS, B. D., (1981). Volume of Fluid (VOF) method for the Dynamics of Free boundaries, *J. Comp. Physics*, 39:201-225.

HOLDEMAN J.D., (1993), Mixing of multiple jets with a confined subsonic crossflow. *Progress in Energy and Combustion Science.*, 19 31–70.

HOLLAND D.J., MARASHDEH Q., MULLER C.R., WANG F., DENNIS J.S., Fan L.S., Gladden L.F., (2009), Comparison of ECVT and MR Measurements of Voidage in a Gas-Fluidized Bed. *Industrial & Engineering Chemistry Research.*, 48 172–181.

HOLLAND D.J., Gladden L.F., (2014), Less is More: How Compressed Sensing is Transforming Metrology in Chemistry. *Angewandte Chemie International Edition.*, 53 13330–13340.

ISMAIL I., GAMIO J.C., BUKHARI S.F.A., YANG W.Q., (2005), Tomography for multi-phase flow measurement in the oil industry. *Flow Measurement and Instrumentation.*, 16 145–155.

ISO/IEC 17025:2005: General requirements for the competence of testing and calibration laboratories

ISO 3171 (1999). Methods of test for petroleum and its products, Petroleum liquids –automatic pipeline sampling, International Standardisation Organisation..

KUMARA W.A.S., HALVORSEN B.M., MELAAE M.C., (2010), Particle image velocimetry for characterizing the flow structure of oil-water flow in horizontal and slightly inclined pipes. *Chemical Engineering Science.*, 65 4332–4349.

LAKSHMANAN S., MARU W., HOLLAND D., SEDERMAN A., (2015), Multiphase flow measurement using Magnetic Resonance Imaging, *7th Int. Symp. in Process Tomography*, 1-3 Sept.

MAHESH K., (2012), The Interaction of Jets with Crossflow. *Ann. Rev. Fluid Mechanics*, (**45**) 379–407.

MARGASON R.J., (1993), *Fifty years of jet in cross flow research, In Computational and Experimental Assessment of Jets in Cross Flow.*, AGARD–CP-534 1-33.

MAUDSLEY A., HILAL S.K., PERMAN W.H., SIMON H.E.,(1983), Spatially resolved high resolution spectroscopy by "four-dimensional" NMR. *Journal of Magnetic Resonance.*, 51 147–152.

NISHIMURA D.G., (2010), Principles of Magnetic Resonance Imaging, www.lulu.com.

NYDAL O., PINTUS S., ANDREUSSI P., (1992), Statistical characterization of slug flow in horizontal pipes. *Int. J. Multiphase Flow.*, 18 439–453.

OpenFOAM: Open Source CFD Toolkit - http://www.openfoam.com/

PACEK A. W., MAN C. C., NIENOW A. W (1998), On the Sauter mean diameter and size distribution in turbulent liquid/liquid dispersion in a stirred vessel, *Chemical Engineering Science*, 53(11):2005-2011.

POTTEN G., WRIGHT S., (2014). Methods of Determining and Verifying Fiscal Sampling System Uncertainity by Analysing 25 Years of Real Field Proving Data and Laboratory Tests Compared with International Acceptance Criteria, *32nd North Sea Flow Measurement Workshop*, 21-24 October.

RENARDY Y., RENARDY M., (2002), PROST: A Parabolic Reconstruction of Surface Tension for the Volume-of-Fluid Method. *Journal of Computational Physics.*, 183 400–421.

SANKEY M., YANG Z., GLADDEN L., JOHNS M.L., LISTER D., NEWLING B., (2009), SPRITE MRI of bubbly flow in a horizontal pipe. *Journal of Magnetic Resonance.*, 199 126–35.

SIMMONS MJH, AZZOPARDI BJ, (2001). Drop size distributions in dispersed liquid-liquid pipe flow, *Int. J. Multiphase Flow*, 27:843-859.

SMITH S.H., MUNGAL M.G., (1998), Mixing, structure and scaling of the jet in crossflow. *Journal of Fluid Mechanics.*, 357 83–122.

TAYLER A.B., HOLLAND D.J., SEDERMAN A.J., GLADDEN L.F., (2012), Applications of ultra-fast MRI to high voidage bubbly flow: measurement of bubble size distributions, interfacial area and hydrodynamics. *Chemical Engineering Science.*, 71 468–483.

TAYLER A.B., HOLLAND D.J., SEDERMAN A.J., GLADDEN L.F., (2011), Time resolved velocity measurements of unsteady systems using spiral imaging. *Journal of Magnetic Resonance.*, 211 1–10.

TRALLERO JL, (1995). Oil-water flow patterns in horizontal pipes, PhD Thesis, Univ. of Tulsa.

UKAS: United Kingdom Accreditation Services - http://www.ukas.com/

VALLE A., (1998). Multiphase pipeline flows in hydrocarbon recovery, *Multiphase Science and Technology*, 10:1-139.

WANG M., (2015), Industrial Tomography: Systems and Applications, Cambridge: Woodhead Publishing.

WANG X., FENG Z., FORNEY LJ.,(1999), Computational simulation of turbulent mixing with mass transfer. *Computers & Structures*, 70 447–465.

XU, X.X., (2007), Study on oil-water two-phase flow in horizontal pipelines. *Journal of Petroleum Science and Engineering.*, 59 43–58.